Multi-Linear Subspace Estimation and Projection for Efficient RFI Excision in SIMO Systems

Tilahun Melkamu Getu[†‡], Wessam Ajib[‡] and Omar A. Yeste-Ojeda[†]
[†]École de Technologie Supérieure (ÉTS), Montréal, QC, Canada
[‡]Université du Québec À Montréal (UQÀM), Montréal, QC, Canada
tilahun-melkamu.getu.1@ens.etsmtl.ca, ajib.wessam@uqam.ca and Omar.Yeste@lassena.etsmtl.ca

***Abstract*—The paper introduces the multi-linear algebra framework to the radio frequency interference (RFI) excision research by proposing a multi-linear subspace estimation and projection (MLSEP) algorithm for efficient RFI excision in single-input multiple-output (SIMO) systems. Thereafter, the paper compares the MLSEP algorithm with the state-of-the-art projection-based RFI excision algorithms. Eventually, Matlab® Monte-Carlo simulations corroborate that MLSEP outperforms the state-of-the-art projection-based RFI excision algorithms.**

***Index Terms*—RFI excision, multi-linear subspace estimation, multi-linear projection, MLSEP, tensor-based signal processing.**

I. Introduction

RFI is generally caused by out-of-band emissions by nearby transmitters and harmonics, jamming, spoofing and meaconing. If left unmitigated, such an RFI can evoke a severe system performance loss both in satellite and terrestrial communications. Consequently, tremendous attention has been paid for RFI detection and excision in different research disciplines.

RFI detection and excision have received immense attention in radio astronomy [1] [2], microwave radiometry [3] [4] and global navigation satellite systems [5] [6]. As a result, spectral [3], temporal [7], spectral-temporal [6], statistical [8] [9] [10], spatial filtering-based [1] [2] and transformed domain-based [11] algorithms have been proposed. Amongst the existing algorithms, subspace projection (SP) [1] and cross subspace projection (CSP) [2] are the state-of-the-art projection-based algorithms proposed for the excision of an RFI emitted by a relatively stationary interferer. To continue, SP relies on the eigen value decomposition (EVD) of the space-time correlation matrix [1]. Whereas auxiliary-antenna assisted CSP relies on the singular value decomposition (SVD) of the space-time cross-correlation matrix [2].

On the other hand, recent advances in tensor-based signal processing [12] [13] have substantiated that tensor-based parameter estimators which deploy truncated higher-order SVD (HOSVD) have outperformed their matrix-based counterparts for the former parameter estimators exploit the inherent structure of the measurement data. Meanwhile, the congestion of licensed spectrum both in satellite and terrestrial communications and the advent of cognitive radios [14] call for efficient signal processing algorithms which can evoke efficient RFI excision.

However, the multi-linear algebra framework has never been investigated to date for efficient RFI excision to the best of the knowledge of the authors, since tensor-based subspace estimators didn't receive much attention till recently. Consequently, this paper introduces the multi-linear algebra framework by proposing a *multi-linear subspace estimation and projection* (MLSEP) algorithm for efficient RFI excision in SIMO systems.

In MLSEP, truncated HOSVD [13] [15] is used to obtain the estimated RFI subspace tensor. No signal of interest (SOI) is transmitted during the estimation of the RFI subspace tensor—analogous to a *pre-look* interval in [16]—of a severe broadband RFI emitted by a stationary interferer. Meanwhile, the estimation of the RFI subspace tensor is pursued similar to the estimation of the signal subspace tensor in [17]. Hereinafter, a multi-linear projector which evokes efficient excision of the RFI is derived based-on the estimated RFI subspace tensor. Following this introduction, the paper is organized as follows. Section II presents the notation and system model. Section III details the MLSEP algorithm. Simulation results are then presented in section IV followed by paper conclusions which are drawn in section V.

II. Notation and System Model

A. Notation

Throughout the paper, scalars, vectors, matrices and tensors are denoted by italic letters, lower-case bold-face letters, upper-case bold-face letters and bold-face calligraphic letters, respectively. The notations $(:,i)$, $||\cdot||_F$, $(\cdot)^T$, $(\cdot)^H$, $\otimes$, $(\cdot)^+$, $(\cdot)^{+r}$ and $\mathbb{E}\{\cdot\}$ imply the ith column of a matrix, Frobenius norm, transposition, Hermitian transposition, Kronecker product, Moore-Penrose pseudo-inverse, the r-mode pseudo-inverse of a tensor and expectation operation, respectively.

The R-dimensional tensor $\boldsymbol{\mathcal{A}} \in \mathbb{C}^{I_1 \times I_2 \times \ldots \times I_R}$ is an R-way array of size I_r along the r-th mode which is consistent with [18]. The r-mode vectors of $\boldsymbol{\mathcal{A}}$ are obtained by varying the rth index, while keeping all other indices fixed and the r-mode unfolding of $\boldsymbol{\mathcal{A}}$ is obtained by collecting all r-mode vectors into a matrix and represented by $[\boldsymbol{\mathcal{A}}]_{(r)} \in \mathbb{C}^{I_r \times I_{r+1} \cdot \ldots \cdot I_R \cdot I_1 \cdot \ldots \cdot I_{r-1}}$. Moreover, the r-rank of $\boldsymbol{\mathcal{A}}$ is defined as the rank of $[\boldsymbol{\mathcal{A}}]_{(r)}$.

The r-mode product of a tensor $\boldsymbol{\mathcal{A}}$ and a matrix $\boldsymbol{U}_r \in \mathbb{C}^{J_r \times I_r}$ is denoted as $\boldsymbol{\mathcal{B}} = \boldsymbol{\mathcal{A}} \times_r \boldsymbol{U}_r$. It is visualized as multiplying the r-mode vectors of $\boldsymbol{\mathcal{A}}$ from left-hand side by the matrix $\boldsymbol{U}_r$, i.e., $[\boldsymbol{\mathcal{B}}]_{(r)} = \boldsymbol{U}_r [\boldsymbol{\mathcal{A}}]_{(r)}$ [15]. Similarly, the r-mode product of a tensor $\boldsymbol{\mathcal{A}} \in \mathbb{C}^{I_1 \times I_2 \times \ldots I_r \times \ldots \times I_R}$ and a tensor $\boldsymbol{\mathcal{C}} \in$

978-1-4799-7591-4/15/$31.00 ©2015 IEEE

$\mathbb{C}^{J_1 \times J_2 \times \ldots J_r \times \ldots \times J_R}$, where $I_r = J_1 J_2 \ldots J_{r-1} J_{r+1} \ldots J_R$, is denoted by $\boldsymbol{\mathcal{D}} = \boldsymbol{\mathcal{A}} \times_r \boldsymbol{\mathcal{C}} \in \mathbb{C}^{I_1 \times \ldots I_{r-1} \times J_r \times I_{r+1} \ldots \times I_R}$ and $[\boldsymbol{\mathcal{D}}]_{(r)} = [\boldsymbol{\mathcal{C}}]_r [\boldsymbol{\mathcal{A}}]_{(r)}$ [19]. Accordingly, the r-mode identity tensor $\boldsymbol{\mathcal{I}}_r \in \mathbb{C}^{J_1 \times J_2 \times \ldots J_r \times \ldots \times J_R}$ as well as the r-mode pseudo-inverse tensor $\boldsymbol{\mathcal{A}}^{+r}$ are defined and satisfy [19]

$$\left(\boldsymbol{\mathcal{A}} \times_r \boldsymbol{\mathcal{A}}^{+r}\right) \times_r \boldsymbol{\mathcal{A}} = \boldsymbol{\mathcal{A}} \text{ and } \boldsymbol{\mathcal{I}}_r \times_r \boldsymbol{\mathcal{A}} = \boldsymbol{\mathcal{A}}, \quad (1)$$

where $[\boldsymbol{\mathcal{A}}^{+r}]_{(r)} = [\boldsymbol{\mathcal{A}}]^{+}_{(r)}$, $[\boldsymbol{\mathcal{I}}]_{(r)} = \boldsymbol{I}_{J_r \times J_{r+1} \ldots J_R J_1 \ldots J_{r-1}}$, $J_r = J_{r+1} \ldots J_R J_1 \ldots J_{r-1}$ and $J_r = I_{r+1} \ldots I_R I_1 \ldots I_{r-1}$.

B. System Model

We consider a SIMO system with N_R receive antennas suffering from a severe broadband RFI emitted by a stationary interferer equipped with a single antenna. We model the SOI channel between the transmitter and each receive antenna pair as a finite-duration impulse response (FIR) filter with $L+1$ taps [20]. Besides, the SOI channel is assumed to be time-invariant for a long-term interval (LTI). Similarly, we model the time-invariant RFI channel between the RFI transmitter and each receive antenna pair as an FIR filter with $L_f + 1$ taps. The received signal at time n would then be

$$\boldsymbol{y}(n) = \sum_{l=0}^{L} \boldsymbol{h}_l s(n-l) + \sum_{l=0}^{L_f} \boldsymbol{g}_l f(n-l) + \boldsymbol{z}(n), \quad (2)$$

where $\{\boldsymbol{h}_l, \boldsymbol{g}_l\} \in \mathbb{C}^{N_R}$ are the array response of the N_R antennas corresponding to the lth SOI and RFI channel taps, respectively, $s(n)$ denotes the symbol emitted by the SOI transmitter at time n, $f(n)$ is the sampled broadband RFI which is usually modeled as a zero mean additive white Gaussian noise (AWGN) [5] and $\boldsymbol{z}(n) \in \mathbb{C}^{N_R}$ is the sampled AWGN with a distribution $\mathcal{N}\big(\boldsymbol{0}, \sigma^2 \boldsymbol{I}_{N_R}\big)$. Furthermore, we assume that the SOI, RFI and AWGN are uncorrelated and perfect estimates of L and L_f are available.

III. MLSEP

The MLSEP algorithm comprises two phases. In the first phase, no SOI is transmitted for a duration of one LTI in order to estimate the projection tensor. One LTI is made of N short-term intervals (STIs). During each STI duration of WT_s for T_s being the symbol duration, W samples from every N_R antennas are stacked and the horizontal concatenation of N stacked STIs forms a matrix. The multi-linear equivalent of such a matrix is deployed to estimate the RFI subspace tensor using truncated HOSVD. Thereafter, the multi-linear projector is derived from the estimated RFI subspace tensor.

In the second phase, SOI is transmitted from the second LTI onwards and a per LTI RFI excision would be executed via the already derived multi-linear projector for the interferer under consideration is stationary.

A. Problem Setup

Stacking the observation vectors of the N_R receive antennas and W data windows into one highly structured vector of size $N_R.W \times 1$ with respect to the mth STI gives

$$\boldsymbol{y}_m = \boldsymbol{H}\boldsymbol{s}_m + \boldsymbol{G}\boldsymbol{f}_m + \boldsymbol{z}_m \in \mathbb{C}^{N_R.W}, \quad (3)$$

where $\boldsymbol{s}_m = \big[s(mW), \ldots, s(mW - W - L + 1)\big]^T \in \mathbb{C}^{(W+L)}$, $\boldsymbol{f}_m = \big[f(mW), \ldots, f(mW - W - L_f + 1)\big]^T \in \mathbb{C}^{(W+L_f)}$ and $\boldsymbol{z}_m \in \mathbb{C}^{N_R.W}$ are the sampled SOI, RFI and zero mean AWGN, respectively. Besides, $\boldsymbol{H} \in \mathbb{C}^{N_R.W \times (W+L)}$ is the SOI filtering matrix as defined in [17] and $\boldsymbol{G} \in \mathbb{C}^{N_R.W \times (W+L_f)}$ is the RFI filtering matrix structured as

$$\boldsymbol{G} = \Big[\boldsymbol{G}_1^T, \boldsymbol{G}_2^T, \ldots, \boldsymbol{G}_{N_R}^T\Big]^T, \quad (4)$$

where $\boldsymbol{G}_j \in \mathbb{C}^{W \times (W+L_f)}$ is a banded Toeplitz matrix associated with the jth receive antenna's RFI impulse response $\boldsymbol{g}_j \triangleq \big[g_j^0, \ldots, g_j^{L_f}\big]^T = \big[g_j(t_0), \ldots, g_j(t_0 + L_f T_s)\big]^T$ and

$$\boldsymbol{G}_j = \begin{bmatrix} g_j^0 & \ldots & g_j^{L_f} & 0 & \ldots & \ldots & 0 \\ 0 & g_j^0 & \ldots & g_j^{L_f} & 0 & \ldots & 0 \\ \vdots & \vdots & \vdots & \vdots & \vdots & \vdots & \vdots \\ 0 & \ldots & \ldots & 0 & g_j^0 & \ldots & g_j^{L_f} \end{bmatrix}. \quad (5)$$

Here t_0 denotes the time-of-arrival. Meanwhile, the horizontal concatenation of N $\boldsymbol{y}_m$s from (3) renders

$$\boldsymbol{Y} = \boldsymbol{H}\boldsymbol{S} + \boldsymbol{G}\boldsymbol{F} + \boldsymbol{Z} \in \mathbb{C}^{N_R.W \times N}. \quad (6)$$

In the first LTI, no SOI is transmitted and the received signal would then be

$$\boldsymbol{Y}_I = \boldsymbol{G}\boldsymbol{F} + \boldsymbol{Z} \in \mathbb{C}^{N_R.W \times N}. \quad (7)$$

The noiseless version of (7) and $\boldsymbol{G}$ span identical column space [21]. However, the AWGN perturbs the singular vectors that span the RFI subspace and the estimated RFI subspace $\hat{\boldsymbol{U}}_I \in \mathbb{C}^{N_R.W \times (W+L_f)}$ for $N_R.W \geq W + L_f$ can be obtained from the SVD of (7) as

$$\boldsymbol{Y}_I = [\hat{\boldsymbol{U}}_I \, \hat{\boldsymbol{U}}_n] \begin{bmatrix} \hat{\boldsymbol{\Sigma}}_I & \boldsymbol{0}_{r \times (N-r)} \\ \boldsymbol{0}_{(N_R.W - r) \times r} & \hat{\boldsymbol{\Sigma}}_n \end{bmatrix} [\hat{\boldsymbol{V}}_I \, \hat{\boldsymbol{V}}_n]^H, \quad (8)$$

where $\hat{\boldsymbol{\Sigma}}_I = \text{diag}(\sigma_1, \sigma_2, \ldots, \sigma_r)$ and $r = W + L_f$.

B. Problem Formulation

If $\big[\boldsymbol{\mathcal{Y}}\big]^T_{(3)}$ should be equal to $\boldsymbol{Y}$ in (6), the multi-linear equivalent of (6) would be

$$\boldsymbol{\mathcal{Y}} = \boldsymbol{\mathcal{H}} \times_3 \boldsymbol{S}^T + \boldsymbol{\mathcal{G}} \times_3 \boldsymbol{F}^T + \boldsymbol{\mathcal{Z}}, \quad (9)$$

where $\boldsymbol{\mathcal{H}} \in \mathbb{C}^{N_R \times W \times (W+L)}$ and $\boldsymbol{\mathcal{G}} \in \mathbb{C}^{N_R \times W \times (W+L_f)}$ are the SOI and RFI filtering tensors constructed by aligning the banded Toeplitz matrices $\boldsymbol{H}_j$ and $\boldsymbol{G}_j$ for $1 \leq j \leq N_R$, respectively, as in Fig. 1, i.e., $[\boldsymbol{\mathcal{H}}]^T_{(3)} = \boldsymbol{H}$ and $[\boldsymbol{\mathcal{G}}]^T_{(3)} = \boldsymbol{G}$, and $\boldsymbol{\mathcal{Z}}$ is the noise tensor. Meanwhile, we assume $\boldsymbol{S}$ has a rank of $W + L$, i.e., $N \geq (W + L)$, $\boldsymbol{F}$ has a rank of $W + L_f$, i.e., $N \geq (W + L_f)$, $[\boldsymbol{\mathcal{H}}]_{(3)}$ has a full row rank, i.e., $N_R.W \geq W + L$, $[\boldsymbol{\mathcal{G}}]_{(3)}$ has a full row rank, i.e., $N_R.W \geq W + L_f$, $W > L$ and $W > L_f$ in order to ensure the identifiability of SOI and RFI subspaces.

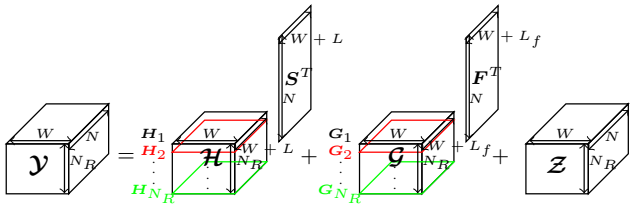

Fig. 1. Multi-linear formulation from the received signal per LTI $\boldsymbol{Y}$ in (6).

1) RFI Subspace Estimation: In the first LTI, no SOI is transmitted and hence the truncated HOSVD of the received signal $\boldsymbol{\mathcal{Y}}_I = \boldsymbol{\mathcal{G}} \times_3 \boldsymbol{F}^T + \boldsymbol{\mathcal{Z}}$ would be [13]

$$\boldsymbol{\mathcal{Y}}_I \approx \hat{\boldsymbol{\mathcal{S}}}^{[I]} \times_1 \hat{\boldsymbol{U}}_1^{[I]} \times_2 \hat{\boldsymbol{U}}_2^{[I]} \times_3 \hat{\boldsymbol{U}}_3^{[I]}, \tag{10}$$

where $\hat{\boldsymbol{\mathcal{S}}}^{[I]} \in \mathbb{C}^{r_1 \times r_2 \times r_3}$ is the core tensor which satisfies the all-orthogonality conditions, $\hat{\boldsymbol{U}}_1^{[I]} \in \mathbb{C}^{N_R \times r_1}$ is a unitary matrix of the singular vectors of $[\boldsymbol{\mathcal{Y}}_I]_{(1)}$, $\hat{\boldsymbol{U}}_2^{[I]} \in \mathbb{C}^{W \times r_2}$ is a unitary matrix of the singular vectors of $[\boldsymbol{\mathcal{Y}}_I]_{(2)}$, $\hat{\boldsymbol{U}}_3^{[I]} \in \mathbb{C}^{N \times r_3}$ is a unitary matrix of the singular vectors of $[\boldsymbol{\mathcal{Y}}_I]_{(3)}$ and r_n denotes the n-rank of the noiseless tensor $\widetilde{\boldsymbol{\mathcal{Y}}}_I$, i.e., $\widetilde{\boldsymbol{\mathcal{Y}}}_I = \boldsymbol{\mathcal{G}} \times_3 \boldsymbol{F}^T$, for $n = 1, 2, 3$ [13] [17]. In our RFI subspace estimation, $r_1 = \min(N_R,\ L_f + 1)$, $r_2 = \min(W,\ N.N_R)$ and $r_3 = \min(N,\ W + L_f)$. Accordingly, $r_2 = W$ and $r_3 = W + L_f$ for the assumption $N \geq W + L_f$. From (10), the estimated RFI subspace tensor $\hat{\boldsymbol{\mathcal{U}}}^{[I]}$ is defined as [13]

$$\hat{\boldsymbol{\mathcal{U}}}^{[I]} = \hat{\boldsymbol{\mathcal{S}}}^{[I]} \times_1 \hat{\boldsymbol{U}}_1^{[I]} \times_2 \hat{\boldsymbol{U}}_2^{[I]} \times_3 \hat{\boldsymbol{\Sigma}}_I^{-1}. \tag{11}$$

Note that the columns of $\left[\hat{\boldsymbol{\mathcal{U}}}^{[I]}\right]_{(3)}^T \in \mathbb{C}^{N_R.W \times r_3}$ span the estimated RFI subspace and inspire the underneath theorem.

Theorem 1: The tensor-based RFI subspace estimator $\left[\hat{\boldsymbol{\mathcal{U}}}^{[I]}\right]_{(3)}^T$ and the matrix-based RFI subspace estimator $\hat{\boldsymbol{U}}_I$ are related by

$$\left[\hat{\boldsymbol{\mathcal{U}}}^{[I]}\right]_{(3)}^T = (\hat{\boldsymbol{T}}_1 \otimes \hat{\boldsymbol{T}}_2)\ .\ \hat{\boldsymbol{U}}_I, \tag{12}$$

where $\hat{\boldsymbol{T}}_r = \hat{\boldsymbol{U}}_r^{[I]}\ .\ \hat{\boldsymbol{U}}_r^{[I]^H}$, $r = 1, 2$.

Proof: Firstly, note that $\hat{\boldsymbol{\Sigma}}_I^{-1}$ has no impact on the RFI subspace estimation accuracy and is included for the sake of the mathematical analysis. Then, deploying the concept of Theorem 1 and Lemma 1 in [13] and using (11), (10) and (8) render the relation. ∎

2) Multi-Linear Projection: For a perfectly estimated RFI subspace tensor $\hat{\boldsymbol{\mathcal{U}}}^{[I]} \in \mathbb{C}^{N_R \times W \times (W+L_f)}$, the multi-linear projector defined beneath evokes perfect excision of the RFI.

Theorem 2: For a perfect $\hat{\boldsymbol{\mathcal{U}}}^{[I]}$, the multi-linear projector $\boldsymbol{\mathcal{P}} \in \mathbb{C}^{N_R \times W \times N_R.W}$ which evokes perfect RFI excision is given by

$$\boldsymbol{\mathcal{P}} = \boldsymbol{\mathcal{I}}_3 - \hat{\boldsymbol{\mathcal{U}}}^{[I]} \times_3 \left(\hat{\boldsymbol{\mathcal{U}}}^{[I]}\right)^{+3}, \tag{13}$$

where $\boldsymbol{\mathcal{I}}_3 \in \mathbb{C}^{N_R \times W \times N_R.W}$ is the 3-mode identity tensor, $\left(\hat{\boldsymbol{\mathcal{U}}}^{[I]}\right)^{+3}$ is the 3-mode pseudo-inverse tensor, $[\boldsymbol{\mathcal{I}}_3]_{(3)} = \boldsymbol{I}_{N_R.W}$ and $\left[\left(\hat{\boldsymbol{\mathcal{U}}}^{[I]}\right)^{+3}\right]_{(3)} = \left[\hat{\boldsymbol{\mathcal{U}}}^{[I]}\right]_{(3)}^{+}$.

Proof: cf. Appendix A. ∎

However, perfect excision is impossible since the RFI subspace estimate cannot be perfect and a performance parameter is sought. If projection matrix $\boldsymbol{P}$ is formed from (8) as $\boldsymbol{P} = \boldsymbol{I}_{N_R.W} - \hat{\boldsymbol{U}}_I \hat{\boldsymbol{U}}_I^H$, perfect RFI excision implies $\left\|\boldsymbol{PG}\right\|_F = 0$ and $\left\|\left[\boldsymbol{\mathcal{P}} \times_3 \boldsymbol{\mathcal{G}}\right]_{(3)}^T\right\|_F^2 = 0$. Consequently, we define a performance parameter named root mean square excision error (RMSEE) which quantizes the root mean square RFI excision error during an LTI as

$$\text{RMSEE} = \sqrt{\mathbb{E}\left\{\left\|\boldsymbol{PG}\right\|_F^2\right\}} \tag{14}$$

$$\text{RMSEE} = \sqrt{\mathbb{E}\left\{\left\|\left[\boldsymbol{\mathcal{P}} \times_3 \boldsymbol{\mathcal{G}}\right]_{(3)}^T\right\|_F^2\right\}}. \tag{15}$$

C. MLSEP Algorithm

Algorithm I: MLSEP for efficient RFI excision in SIMO systems

Input: $\boldsymbol{Y}_I$, $\boldsymbol{Y}$, N_R, W, L, L_f, N

Assumptions: $N \succeq \{W + L, W + L_f\}$, $W \succ \{L, L_f\}$,

Initialization: $r_1 = \min(N_R,\ L_f + 1)$, $r_2 = \min(W,\ N.N_R)$

$\boldsymbol{\mathcal{Y}}_I$ =the tensorization of $\left[\boldsymbol{\mathcal{Y}}_I\right]_{(3)} = \boldsymbol{Y}_I^T$

$[\boldsymbol{\mathcal{Y}}_I]_{(1)} = \boldsymbol{U}_1 \boldsymbol{\Sigma}_1 \boldsymbol{V}_1^H$; $\hat{\boldsymbol{U}}_1^{[I]} = \boldsymbol{U}_1(:, 1 : r_1)$

$[\boldsymbol{\mathcal{Y}}_I]_{(2)} = \boldsymbol{U}_2 \boldsymbol{\Sigma}_2 \boldsymbol{V}_2^H$; $\hat{\boldsymbol{U}}_2^{[I]} = \boldsymbol{U}_2(:, 1 : r_2)$

$\boldsymbol{Y}_I = \boldsymbol{U} \boldsymbol{\Sigma} \boldsymbol{V}^H$; $\hat{\boldsymbol{U}}_I = \boldsymbol{U}(:, 1 : W + L_f)$

$\left[\hat{\boldsymbol{\mathcal{U}}}^{[I]}\right]_{(3)}^T = \left(\hat{\boldsymbol{T}}_1 \otimes \hat{\boldsymbol{T}}_2\right)\ .\ \hat{\boldsymbol{U}}_I$; $\hat{\boldsymbol{T}}_r = \hat{\boldsymbol{U}}_r^{[I]}\ .\ \hat{\boldsymbol{U}}_r^{[I]^H}$, $r = 1, 2$

$\hat{\boldsymbol{\mathcal{U}}}^{[I]}$ = the tensorization of $\left[\hat{\boldsymbol{\mathcal{U}}}^{[I]}\right]_{(3)}$

$\boldsymbol{\mathcal{P}} = \boldsymbol{\mathcal{I}}_3 - \hat{\boldsymbol{\mathcal{U}}}^{[I]} \times_3 \left(\hat{\boldsymbol{\mathcal{U}}}^{[I]}\right)^{+3} \in \mathbb{C}^{N_R \times W \times N_R.W}$

Repeat

$\boldsymbol{\mathcal{Y}}$ =the tensorization of $\left[\boldsymbol{\mathcal{Y}}\right]_{(3)} = \boldsymbol{Y}^T$

return $\left[\boldsymbol{\mathcal{P}} \times_3 \boldsymbol{\mathcal{Y}}\right]_{(3)}^T$

Until no SOI transmission

IV. Simulation Results

During the first LTI, we transmitted a zero mean AWGN—which models the broadband RFI—over a multipath fading channel. From the second LTI onwards, we transmitted both Gray-coded 4-QAM symbols as an SOI and a broadband RFI over multipath fading channels for $N_{\text{SOI}} = 200$ LTIs. To simulate the SOI and RFI multipath fading channels, $(L+1)$- and (L_f+1)-ray multipath continuous-time channels are constructed synchronously using the raised cosine pulse shaping filter $p_{rc}(t, \beta)$ with a roll-off factor of $\beta = 0.5$ and propagation delay $t_0 = 0.1T_s$ as in [17] [22].

Having taken the EVD of the space-time correlation matrix made of (3), the dominant eigenvectors are used for the simulation of the SP algorithm [1]. On the otherhand, (3) and the version of (3) received via N_R^a low-gain auxiliary antennas make the space-time cross-correlation matrix whose SVD is

Algorithms	Single-path ($L+1=L_f+1=1$) scenario					Multi-path ($L+1=L_f+1=2$) scenario				
	INR [dB]					INR [dB]				
	0	10	20	30	40	0	10	20	30	40
Perfect excision	2.80 dB	10.21 dB	19.84 dB	29.80 dB	39.80 dB	2.92 dB	10.35 dB	19.95 dB	29.91 dB	39.92 dB
SP [1]	1.35 dB	8.11 dB	17.67 dB	27.62 dB	37.61 dB	1.31 dB	7.62 dB	17.02 dB	26.96 dB	36.96 dB
CSP [2]	1.55 dB	8.18 dB	17.66 dB	27.63 dB	37. 65 dB	1.48 dB	7.76 dB	17.09 dB	27.01 dB	36.99 dB
MLSEP	2.67 dB	10.11 dB	19.74 dB	29.69 dB	39.69 dB	1.87 dB	9.12 dB	18.80 dB	28.76 dB	38.76

TABLE I

AVERAGE SINR GAIN [DB] EVOKED BY PERFECT EXCISION, SP [1], CSP [2] AND MLSEP FOR BOTH SINGLE-PATH AND MULTI-PATH SCENARIOS DURING $N_{\text{SOI}} = 200$ LTIS AND 40 OBSERVED SYMBOLS PER LTI AT $W = 4$, $N = 10$, $\alpha = 100$ AND A PRE-EXCISION SINR OF 0 DB.

used for the simulation of the CSP algorithm [2]. Low-gain auxiliary antennas exhibit large sidelobes where interference is observed at and hence any weak received interference would get strong. To simulate this phenomenon, we deployed an α factor which evokes high interference-to-noise ratio (INR). Meanwhile, MLSEP is simulated as per Algorithm I and the succeeding simulation setup has been deployed.

Both $\boldsymbol{H}$ and $\boldsymbol{G}$ are normalized to a Frobenius norm of $\sqrt{W}$, signal-to-interference-plus-noise ratio (SINR) is defined as $\gamma(\boldsymbol{P}) = 10\log_{10}\frac{\mathbb{E}\left\{\left\|\boldsymbol{PHS}\right\|_F^2\right\}}{\mathbb{E}\left\{\left\|\boldsymbol{PGF}\right\|_F^2\right\}+\mathbb{E}\left\{\left\|\boldsymbol{PZ}\right\|_F^2\right\}}$ and the average SINR gain [dB] is defined as $\frac{1}{N_{\text{SOI}}}\sum_{n=1}^{N_{\text{SOI}}}\left(\gamma(\boldsymbol{P})-\gamma(\boldsymbol{I}_{N_R.W})\right)$. Here note that $\boldsymbol{P} = \left[\boldsymbol{\mathcal{P}}\right]_{(3)}^T$ for MLSEP. Similarly, INR [dB] is defined as $10\log_{10}\frac{\mathbb{E}\left\{\left\|\boldsymbol{GF}\right\|_F^2\right\}}{\mathbb{E}\left\{\left\|\boldsymbol{Z}\right\|_F^2\right\}}$, average RMSEE is simulated by averaging (14) over 200 LTIs for SP and CSP and by averaging (15) over 200 LTIs for MLSEP. Meanwhile, Tensorlab [23] is deployed for our matricization and tensorization operations. Eventually, Monte-Carlo simulations over 1000 channel realizations produce Fig. 2 and Table I.

Fig. 2 showcases MLSEP outperforming both SP and CSP for single- as well as multi-path scenarios. Such a significant performance improvement is attributed to the RFI subspace estimation improvement rendered by the tensor framework.

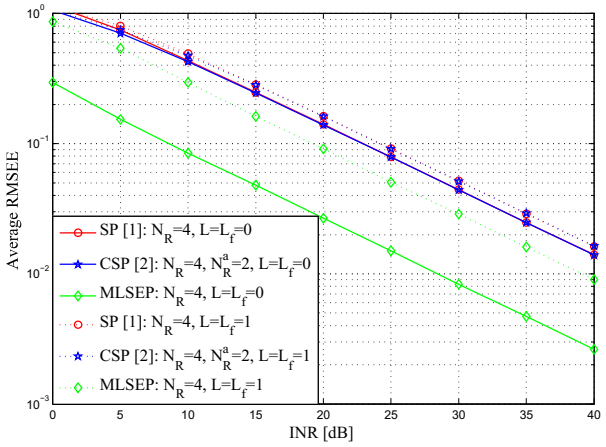

Fig. 2. Average RMSEE for an RFI excision using SP, CSP and MLSEP during $N_{\text{SOI}} = 200$ LTIs and 40 observed symbols per LTI at $W = 4$, $N = 10$, $\alpha = 100$ and a pre-excision SINR of 0 dB.

Meanwhile, the aforementioned improvement is translated to a formidable average SINR gain in Table I. As it is evident in Table I, MLSEP performs close to the perfect excision algorithm which assumes perfect knowledge of the RFI channel.

V. CONCLUSIONS

This paper introduces the multi-linear algebra framework to the RFI excision research. To do so, truncated HOSVD is deployed to estimate the RFI subspace tensor. Thereafter, the *multi-linear projector* that renders perfect excision of the RFI for the perfectly estimated RFI subspace tensor is derived. However, perfect estimate of the RFI subspace tensor cannot be obtained and a performance parameter named RMSEE is defined. Meanwhile, the MLSEP algorithm is proposed of the aforementioned *multi-linear subspace estimation and projection*. Lastly, Monte-Carlo simulations have corroborated that MLSEP outperforms both SP and CSP.

APPENDIX A
PROOF OF THEOREM 2

Proof: For a perfect $\hat{\boldsymbol{\mathcal{U}}}^{[I]}$, the RFI in (9) would be perfectly removed via $\boldsymbol{\mathcal{P}} \in \mathbb{C}^{N_R \times W \times N_R.W}$ iff

$$\boldsymbol{\mathcal{P}} \times_3 \hat{\boldsymbol{\mathcal{U}}}^{[I]} = \boldsymbol{\mathcal{P}} \times_3 \boldsymbol{\mathcal{G}} = \hat{\boldsymbol{\mathcal{U}}}^{[I]} - \hat{\boldsymbol{\mathcal{U}}}^{[I]} = \boldsymbol{\mathcal{O}}_t, \tag{16}$$

where $\boldsymbol{\mathcal{O}}_t \in \mathbb{C}^{N_R \times W \times (W+L_f)}$ is a zero tensor. From (1), $\left(\hat{\boldsymbol{\mathcal{U}}}^{[I]} \times_3 \left(\hat{\boldsymbol{\mathcal{U}}}^{[I]}\right)^{+3}\right) \times_3 \hat{\boldsymbol{\mathcal{U}}}^{[I]} = \hat{\boldsymbol{\mathcal{U}}}^{[I]}$ and $\boldsymbol{\mathcal{I}}_3 \times_3 \hat{\boldsymbol{\mathcal{U}}}^{[I]} = \hat{\boldsymbol{\mathcal{U}}}^{[I]}$, respectively, for $r = 3$ and $[\boldsymbol{\mathcal{I}}_3]_{(3)} = \boldsymbol{I}_{N_R.W}$. Accordingly, perfect excision is possible iff

$$\boldsymbol{\mathcal{P}} \times_3 \hat{\boldsymbol{\mathcal{U}}}^{[I]} = \boldsymbol{\mathcal{I}}_3 \times_3 \hat{\boldsymbol{\mathcal{U}}}^{[I]} - \left(\hat{\boldsymbol{\mathcal{U}}}^{[I]} \times_3 \left(\hat{\boldsymbol{\mathcal{U}}}^{[I]}\right)^{+3}\right) \times_3 \hat{\boldsymbol{\mathcal{U}}}^{[I]} = \boldsymbol{\mathcal{O}}_t. \tag{17}$$

Applying the definition of r-mode product for two tensors highlighted in Section II and the distributive property of matrix product to (17) results in

$$\left[\boldsymbol{\mathcal{P}} \times_3 \hat{\boldsymbol{\mathcal{U}}}^{[I]}\right]_{(3)} = \left[\hat{\boldsymbol{\mathcal{U}}}^{[I]}\right]_{(3)} \left(\left[\boldsymbol{\mathcal{I}}_3\right]_{(3)} - \left[\hat{\boldsymbol{\mathcal{U}}}^{[I]} \times_3 \left(\hat{\boldsymbol{\mathcal{U}}}^{[I]}\right)^{+3}\right]_{(3)}\right). \tag{18}$$

Thereafter, the tensorization of (18) renders

$$\boldsymbol{\mathcal{P}} \times_3 \hat{\boldsymbol{\mathcal{U}}}^{[I]} = \left(\boldsymbol{\mathcal{I}}_3 - \hat{\boldsymbol{\mathcal{U}}}^{[I]} \times_3 \left(\hat{\boldsymbol{\mathcal{U}}}^{[I]}\right)^{+3}\right) \times_3 \hat{\boldsymbol{\mathcal{U}}}^{[I]}. \tag{19}$$

Eventually, equating the LHS and RHS of (19) results in

$$\boldsymbol{\mathcal{P}} = \boldsymbol{\mathcal{I}}_3 - \hat{\boldsymbol{\mathcal{U}}}^{[I]} \times_3 \left(\hat{\boldsymbol{\mathcal{U}}}^{[I]}\right)^{+3}. \tag{20}$$

■

REFERENCES

[1] S. van der Tol and A.-J. van der Veen, "Performance analysis of spatial filtering of RF interference in radio astronomy," *IEEE Trans. Signal Process.*, vol. 53, no. 3, pp. 896–910, Mar. 2005.

[2] B. Jeffs, L. Li, and K. F. Warnick, "Auxiliary antenna-assisted interference mitigation for radio astronomy arrays," *IEEE Trans. Signal Process.*, vol. 53, no. 2, pp. 439–451, Feb. 2005.

[3] B. Guner, J. Johnson, and N. Niamsuwan, "Time and frequency blanking for radio-frequency interference mitigation in microwave radiometry," *IEEE Trans. Geosci. Remote Sens.*, vol. 45, no. 11, pp. 3672–3679, Nov. 2007.

[4] S. Misra, P. Mohammed, B. Guner, C. Ruf, J. Piepmeier, and J. Johnson, "Microwave radiometer radio-frequency interference detection algorithms: A comparative study," *IEEE Trans. Geosci. Remote Sens.*, vol. 47, no. 11, pp. 3742–3754, Nov. 2009.

[5] M. Wildemeersch and J. Fortuny-Guasch, "Radio frequency interference impact assessment on global navigation satellite systems," EC Joint Research Centre, Security Tech. Assessment Unit, Tech. Rep., Jan. 2010.

[6] D. Borio, L. Camoriano, S. Savasta, and L. Lo Presti, "Time-frequency excision for GNSS applications," *IEEE Syst. J.*, vol. 2, no. 1, pp. 27–37, Mar. 2008.

[7] J. T. Johnson and S. W. Ellingson, "Examination of a simple pulse blanking technique for RFI mitigation," *Radio Sci.*, 2005.

[8] C. Ruf, S. Gross, and S. Misra, "RFI detection and mitigation for microwave radiometry with an agile digital detector," *IEEE Trans. Geosci. Remote Sens.*, vol. 44, no. 3, pp. 694–706, Mar. 2006.

[9] J. Arribas, C. Fernandez-Prades, and P. Closas, "Antenna array based GNSS signal acquisition for interference mitigation," *IEEE Trans. Aerosp. Electron. Syst.*, vol. 49, no. 1, pp. 223–243, Jan. 2013.

[10] ——, "Multi-antenna techniques for interference mitigation in GNSS signal acquisition," *EURASIP Journal on Advances in Signal Processing*, vol. 2013, no. 1, 2013. [Online]. Available: http://dx.doi.org/10.1186/1687-6180-2013-143

[11] F. Dovis, L. Musumeci, N. Linty, and M. Pini, "Recent trends in interference mitigation and spoofing detection," *Int. J. of Embedded and Real-Time Communication Systems*, vol. 3, no. 3, pp. 1–17, July-Sept. 2012.

[12] F. Roemer, "Advanced algebraic concepts for efficient multi-channel signal processing," Ph.D. dissertation, Ilmenau Univ. of Tech., 2012.

[13] F. Roemer, M. Haardt, and G. Del Galdo, "Analytical performance assessment of multi-dimensional matrix- and tensor-based ESPRIT-type algorithms," *IEEE Trans. Signal Process.*, vol. 62, no. 10, pp. 2611–2625, May 2014.

[14] S. Haykin, "Cognitive radio: brain-empowered wireless communications," *IEEE J. Sel. Areas Commun.*, vol. 23, no. 2, pp. 201–220, Feb. 2005.

[15] M. Haardt, F. Roemer, and G. Del Galdo, "Higher-order SVD-based subspace estimation to improve the parameter estimation accuracy in multidimensional harmonic retrieval problems," *IEEE Trans. Signal Process.*, vol. 56, no. 7, pp. 3198–3213, July 2008.

[16] H. Subbaram and K. Abend, "Interference suppression via orthogonal projections: a performance analysis," *IEEE Trans. Antennas Propag.*, vol. 41, no. 9, pp. 1187–1194, Sept. 1993.

[17] B. Song, F. Roemer, and M. Haardt, "Blind estimation of SIMO channels using a tensor-based subspace method," in *Proc. the 44th Asilomar Conf. on Signals, Systems and Computers*, Nov. 2010, pp. 8–12.

[18] L. D. Lathauwer, B. D. Moor, and J. Vandewalle, "A multilinear singular value decomposition," *SIAM J. Matrix Anal. Appl*, vol. 21, pp. 1253–1278, 2000.

[19] M. Vasilescu and D. Terzopoulos, "Multilinear projection for appearance-based recognition in the tensor framework," in *Proc. IEEE Int. Conf. on Comput. Vision (IEEE ICCV)*, Oct. 2007, pp. 1–8.

[20] S. Haykin, *Adaptive Filter Theory*, 3rd ed. Prentice-Hall, Inc., 1996.

[21] G. Strang, *Introduction to Linear Algebra*, 3rd ed. Wellesley-Cambridge Press, 2003.

[22] E. Moulines, P. Duhamel, J. Cardoso, and S. Mayrargue, "Subspace methods for the blind identification of multichannel FIR filters," *IEEE Trans. Signal Process.*, vol. 43, no. 2, pp. 516–525, Feb. 1995.

[23] L. Sorber, M. V. Barel, and L. D. Lathauwer, "Tensorlab v2.0," Jan. 2014. [online]. Available: http://www.tensorlab.net/.